Progress In Electromagnetics Research, Vol. 142, 159–188, 2013

SEMI-ANALYTICAL SOLUTIONS OF THE 3-D HOMOGENEOUS HELMHOLTZ EQUATION BY THE METHOD OF CONNECTED LOCAL FIELDS

Hung-Wen Chang* **and Sin-Yuan Mu**

Department of Photonics, National Sun Yat-sen University, Kaohsiung 80424, Taiwan, R.O.C.

Abstract—We advance the theory of the two-dimensional method of connected local fields (CLF) to the three-dimensional cases. CLF is suitable for obtaining semi-analytical solutions of Helmholtz equation. The fundamental building block (cell) of the 3-D CLF is a cube consisting of a central point and twenty six points on the cube's surface. These surface points form three symmetry groups: six on the planar faces, twelve on the edges and eight on the vertices (corners). The local field within the unit cell is expanded in a truncated spherical Fourier-Bessel series. From this representation we develop a closed-form, 3D local field expansion (LFE) coefficients that relate the central point to its immediate neighbors. We also compute the CLF-based FD-FD numerical solutions of the 3D Green's function in free space. Compared with the analytic solution, we found that even at a low three points per wavelength spatial sampling, the accumulated phase errors of the CLF 3D Green's function after propagating a distance of ten wavelengths are well under ten percent.

1. INTRODUCTION

Frequency-domain finite-difference (FD-FD) methods using the classical second-order accurate scheme have been successfully applied to analyze some passive optical waveguide devices [1, 2]. Classical FD methods are easy to understand and simple to implement on digital computers, but they have poor numerical dispersion characteristics [3, 4]. Recent advancements in highly accurate 2D FDFD algorithms [5–9] have overcome dispersion problems of the classical methods. Along these lines in 2010 Chang and Mu published

Received 9 June 2013, Accepted 19 August 2013, Scheduled 25 August 2013

* Corresponding author: Hung-Wen Chang (hchang@faculty.nsysu.edu.tw).

work on the method of connected local fields (CLF, [10, 11]). The two-dimensional CLF method provides alternative semi-analytical solutions to the 2D Helmholtz equation. At the time we were unaware that the LFE-9 formulation was identical to the equation given earlier in 2002 by Hadley who chose a humble title [6] for his great work. The main difference between our work and Dr. Hadley's is that we analytically derived both the local LFE error and the global CLF dispersion error equations and proved that this LFE-9 equation is of the sixth-order accuracy, which is theoretically the highest order of accuracy on a nine-point compact stencil [12] for the 2D discrete Helmholtz operator. In addition, we also analytically derived the Fourier-Bessel reconstruction formula for constructing the continuous field from its 2D discrete sampling of the field. For dielectric media with discontinuous interfaces, Dr. Hadley derived a modified compact nine-point stencils for two special cases when the fundamental 3 by 3 grid is divided equally by a horizontal/vertical interface [1] and when there is a right angle corner in the cell [7]. We are also developing other special compact stencils to make CLF a viable modeling tool for studying practical complex waveguide structures.

Under the 2D method of the connected local fields, the entire solution is made of overlapping or interlocking local fields. Each square-shape local field centered on a given point is composed of a truncated Fourier-Bessel (FB) series. Furthermore, these FB coefficients are algebraically related to the eight points on the corner and the boundary of a square. In other words, the field in the center can be written as the weight sum over the eight fields on the square. Hence, instead of solving the much larger matrix equation for coupled truncated FB series we may solve for the reduced matrix equation for these coupled fields. The end result is that solving for the overlapping local fields is just like solving for any 2D FD-FD equation with a compact nine point stencil. The main benefit of CLF formulation over classical FD-FD methods is the significant cost saving in both the processing time and semiconductor memory. Furthermore, with little computational effort via the analytical LFE reconstruction formula, we are able to obtain higher sampling of the field solution using a lesser CLF sampling density.

There is a tremendous gain in reducing the computational cost if one may use a coarser mesh size in any 3D computation. Over the past decade, few attempts were made to construct better discrete formulas for 3-D Helmholtz equation that would generate very little numerical dispersion. Sutmann proposed the improved FD-like scheme for discretizing 3-D Helmholtz equation with source term in an uniform region [13]. For convenience, Sutmann's scheme is named FD3D-

6-27, in which the first number denotes the order of accuracy and the second denotes the total number of the involved points within a fundamental cube. Similarly, Fernandes and Loula also proposed a sixth-order accurate, quasi optimal finite difference method for Helmholtz problem [14] in three dimensions. Their coefficients are obtained numerically by minimizing a least-squares functional of the local truncation error for plane wave solutions in any direction. In this paper we advance the work of the method of connected local fields (CLF) to the 3-D homogeneous case. For the 3-D homogeneous Helmholtz equation, we expand the local field at a given point by spherical Fourier-Bessel series (SFB) and through an elaborated process, derive the sixth-order accurate analytical formulation, called LFE3D-27. The result was first presented in December 2012 at an international photonic conference [15]. Like the 2D case, this LFE3D-27 formulation is structurally equivalent to a twenty-seven point 3D FD-FD compact stencil.

2. LITERATURE REVIEW

In this session, we quickly review certain newly-developed improved FD-like schemes for discretizing 3-D Helmholtz equation in the past decade. The 3-D homogeneous Helmholtz equation is given by

$$\left(\nabla^2 + k^2\right) u\left(\bar{r}\right) = 0. \tag{1}$$

In Eq. (1), $\bar{r}$ is position vector, ∇^2 represents the Laplace operator, and k denotes wavenumber. Following the logic for 2D CLF, we aim to discretize Eq. (1). Fig. 1 shows the basic cubic structure for a 3D uniformly sampled space (grid size equals Δ in each direction). Out of the total 27 sampled-points (nodes, control points) there are four groups with various symmetry properties:

- A central node: we denote the field on it by u_0.
- Six face-centered nodes: we denote summation of these fields by u_Σ^f.
- Twelve edge-centered nodes: we denote summation of these fields as u_Σ^e.
- Eight corner nodes: we represent the summation of these fields by u_Σ^c.

We seek the 3D local field expansion coefficients that would lead to a compact 27-point FD-like stencil for discretizing 3-D Helmholtz equation. From a symmetry consideration we expect the general expression of this equation to be written as:

$$W_f\, u_\Sigma^f + W_e\, u_\Sigma^e + W_c\, u_\Sigma^c - W_0 u_0 = 0, \tag{2a}$$

where

$$u_{\Sigma}^{f} \triangleq u_{+00} + u_{-00} + u_{0+0} + u_{0-0} + u_{00+} + u_{00-}, \tag{2b}$$

$$u_{\Sigma}^{e} \triangleq u_{++0} + u_{-+0} + u_{+-0} + u_{--0} + u_{+0+} + u_{+0-} + u_{-0+} + u_{-0-} + u_{0++} + u_{0-+} + u_{0+-} + u_{0--}, \tag{2c}$$

and

$$u_{\Sigma}^{c} \triangleq u_{+++} + u_{++-} + u_{+-+} + u_{+--} + u_{-++} + u_{-+-} + u_{--+} + u_{---}. \tag{2d}$$

Here each subscript contains three symbols corresponding to the x, y or z location. Each symbol can be a plus, a minus or a zero sign indicating the amount of displacement in units of grid spacing Δ along the x, y or z direction.

Various FD-like formulae corresponding to different combinations of coefficients W_f, W_e, W_c, and W_0 have been investigated. We first review several important FD-like formulae for discretizing 3-D Helmholtz equation including the classical FD schemes and improved FD-like formulae.

2.1. Classical FD Formula: FD3D-2-7

Standard discrete Helmholtz form (SDHF) means direct discretization of the Helmholtz operator of Eq. (1). It can be obtained by directly applying a finite difference approximation to the partial differential operators. For the classical SDHF, Laplace operator in Eq. (1) is replaced by the classical second-order accurate seven-point formula [16], Eq. (1) is discretized as:

$$W_f = \frac{1}{\Delta^2}, \;\; W_e = 0, \;\; W_c = 0, \;\; W_0 = \frac{6}{\Delta^2} - k^2. \quad \text{(FD3D-2-7)} \tag{3}$$

This second-order accurate 3D FD stencil involves a total of 7 points is called FD3D2-7 in which the first number denotes the order of accuracy and the second denotes the number of considered points within a fundamental cube. We learn from previous dispersion analysis [17] that solving problems with the FD2D-2-7 approximation requires more than twenty sampling points per wavelength to reduce the numerical dispersion error to less than 1% per single wavelength propagation distance. Thus we seek for better approximations.

2.2. Classical FD Formula: FD3D-2-27

When we consider using all 27 sampling fields in the basic cube, the discrete Laplace operator can be derived in a similar way as the second-order accurate seven-point formula [18]. After replacing the Laplace

operator in Eq. (1) with the 27-point discrete Laplace operator, we obtain:

$$\begin{aligned} W_f &= \frac{7}{15\Delta^2}, \quad W_e = \frac{1}{10\Delta^2}, \quad W_c = \frac{1}{30\Delta^2}, \\ W_0 &= \frac{64}{15\Delta^2} - k^2. \quad \text{(FD3D-2-27)} \end{aligned} \tag{4}$$

2.3. Nehrbass-Jevtic-Lee's Formula: RD-FD

In 1998, Nehrbass, Jevtic, and Lee improved the FD3D-27 formula and derived a new numerical scheme called RD-FD [19]. It reduced the dispersion error to one half of the classical formula, while maintaining the same order (second-order) of accuracy. Their work contains 1-D, 2-D and 3-D cases and the formula in the 3D case is given by:

$$W_f = 1, \;\; W_e = 0, \;\; W_c = 0, \;\; W_0 = 6j_0(V), \;\; V = k\Delta. \quad \text{(RD-FD)} \tag{5}$$

In Eq. (5), $V = k\Delta$, defined as the normalized frequency. The RD-FD formulation is the same as our simple 2D CLF form, the LFE3D-7 [10].

2.4. Sutmann's Formula: FD3D-6-27

Interestingly enough, the Possion equation had a six-order accurate FD approximation [18] 10 years before the Helmholtz equation attained its six-order formulae. In 2006, using the information from Helmholtz equation itself, Singer and Turkel derived the sixth-order accurate scheme for 2-D Helmoltz equation [9]. Sutmann also derived and published in 2007 the sixth-order accurate FD-like formula for the 3-D case [13] and the stencils are given by:

$$\begin{aligned} W_f &= \frac{7}{15\Delta^2}\left(1 - \frac{V^2}{21}\right), \\ W_e &= \frac{1}{10\Delta^2}\left(1 + \frac{V^2}{18}\right), \quad W_c = \frac{1}{30\Delta^2}, \qquad \text{(FD3D-6-27)} \\ W_0 &= \frac{64}{15\Delta^2}\left(1 - \frac{V^2}{4} - \frac{5V^4}{256} - \frac{V^6}{1536}\right), \quad V = k\Delta. \end{aligned} \tag{6}$$

We will compare these formulations with our LFE-based equations later in the numerical simulation section.

3. DERIVATION OF LFE3D-27 FORMULA

Using a different approach from Sutmann, Fernandes and Loula, we begin our derivation of LFE3D-27 formula by expressing the solution

of Eq. (1) in a spherical coordinate system:

$$\frac{1}{r^2}\frac{\partial}{\partial r}\left(r^2\frac{\partial u}{\partial r}\right)+\frac{1}{r^2\sin\theta}\frac{\partial}{\partial\theta}\left(\sin\theta\frac{\partial u}{\partial\theta}\right)+\frac{1}{r^2\sin^2\theta}\frac{\partial^2 u}{\partial\phi^2}+k^2u=0. \quad (7a)$$

The general solution of Eq. (7a) is the well-known spherical Fourier-Bessel series given by:

$$u(r,\theta,\phi)=a_0^0 j_0(kr)+\sum_{\ell=1}^{\infty} j_\ell(kr)\sum_{m=0}^{\ell} P_\ell^m(\cos\theta)(a_\ell^m\cos m\phi+b_\ell^m\sin m\phi). \quad (7b)$$

3.1. Simple 3-D CLF Formulae from Three Groups

One of the methods to obtain LFE2D-9 equation is to solve the 8-by-8 linear equation which connects the truncated Fourier-Bessel series with the eight surrounding points on the boundary of the basic square patch. The other method is derive the LFE2D-9 equation by considering the optimal linear combination of two LFE-5s equations along the plus and the cross coordinated so that the local error is minimized. Before deriving the LFE3D-27 equation we will examine three simple local field expansion formulae. They are derived by considering the contribution of each symmetry group given in Fig. 1. In the process we shall also obtain local truncation errors for each group. Finally we shall derive the LFE3D-27 formula with the linear combination of these three equations that minimize the local error.

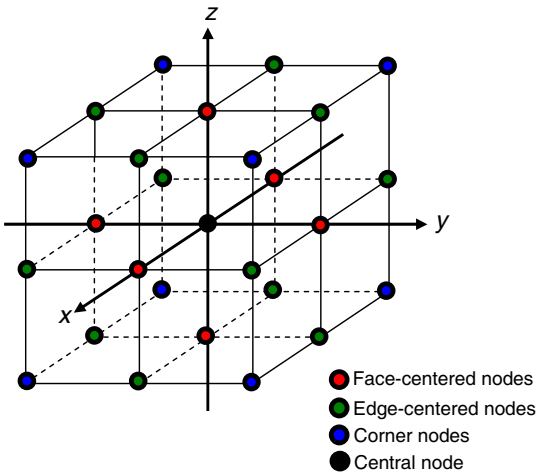

Figure 1. Basic cube and the 27 associated points for the 3D CLF.

3.1.1. Step 1: LFE3D-07 (Face-centered LFE)

As demonstrated in Eqs. (2)–(7), which list all 3D compact FD-FD formulae, these 3D stencils have identical coefficients for the points on faces, edges and corners. Hence we need to consider the expression for summation of wave fields for the face-centered, edge-centered and corner groups. First we consider the face-centered field using Eq. (7b), we have:

$$u_{+00} = u(\Delta,0,0) = u_0 j_0(k\Delta) + \sum_{\ell=1}^{\infty} j_\ell(k\Delta) \sum_{m=0}^{\ell} [P_\ell^m(0)\, a_\ell^m], \tag{8a}$$

$$u_{-00} = u(-\Delta,0,0) = u_0 j_0(k\Delta) + \sum_{\ell=1}^{\infty} j_\ell(k\Delta) \sum_{m=0}^{\ell} [(-1)^m P_\ell^m(0) a_\ell^m], \tag{8b}$$

$$u_{0+0} = u_0 j_0(k\Delta) + \sum_{\ell=1}^{\infty} j_\ell(k\Delta) \left\{ \begin{array}{l} \sum\limits_{m=0}^{\left[\frac{\ell-1}{4}\right]} \left[P_\ell^{4m+1}(0)\, b_\ell^{4m+1}\right] + \sum\limits_{m=0}^{\left[\frac{\ell-2}{4}\right]} \left[(-1) P_\ell^{4m+2}(0)\, a_\ell^{4m+2}\right] \\ + \sum\limits_{m=0}^{\left[\frac{\ell-3}{4}\right]} \left[(-1) P_\ell^{4m+3}(0)\, b_\ell^{4m+3}\right] + \sum\limits_{m=0}^{\left[\frac{\ell}{4}\right]} \left[P_\ell^{4m}(0)\, a_\ell^{4m}\right] \end{array} \right\}, \tag{9a}$$

$$u_{0-0} = u_0 j_0(k\Delta) + \sum_{\ell=1}^{\infty} j_\ell(k\Delta) \left\{ \begin{array}{l} \sum\limits_{m=0}^{\frac{\ell-1}{4}} \left[(-1) P_\ell^{4m+1}(0)\, b_\ell^{4m+1}\right] + \sum\limits_{m=0}^{\frac{\ell-2}{4}} \left[(-1) P_\ell^{4m+2}(0)\, a_\ell^{4m+2}\right] \\ + \sum\limits_{m=0}^{\frac{\ell-3}{4}} \left[P_\ell^{4m+3}(0)\, b_\ell^{4m+3}\right] + \sum\limits_{m=0}^{\frac{\ell}{4}} \left[P_\ell^{4m}(0)\, a_\ell^{4m}\right] \end{array} \right\}, \tag{9b}$$

$$u_{00+} = u_0 j_0(k\Delta) + \sum_{\ell=1}^{\infty} j_\ell(k\Delta)\, a_\ell^0. \tag{10a}$$

$$u_{00-} = u_0 j_0(k\Delta) + \sum_{\ell=1}^{\infty} (-1)^\ell j_\ell(k\Delta)\, a_\ell^0. \tag{10b}$$

Here we use the Gauss bracket symbol $[x]$ to denote the integer part of x.

By summing up Eqs. (8a)–(10b), we have the contributions of all six face-centered fields toward the central point u_0. The result is:

$$u_{\Sigma}^{f} = 6u_0 j_0(k\Delta) + 2\sum_{\ell=1}^{\infty} j_{\ell}(k\Delta) \sum_{m=0}^{\left[\frac{\ell}{2}\right]} \left[P_{\ell}^{2m}(0)\, a_{\ell}^{2m}\right] + 2\sum_{\ell=1}^{\infty} j_{2\ell}(k\Delta)\, a_{2\ell}^{0}$$
$$+2\sum_{\ell=1}^{\infty} j_{\ell}(k\Delta) \left\{ \sum_{m=0}^{\left[\frac{\ell-2}{4}\right]} \left[(-1)\, P_{\ell}^{4m+2}(0)\, a_{\ell}^{4m+2}\right] + \sum_{m=0}^{\left[\frac{\ell}{4}\right]} \left[P_{\ell}^{4m}(0)\, a_{\ell}^{4m}\right] \right\}. \tag{11}$$

We can further simplify Eq. (11) by considering the following properties of associated Legendre polynomials:

$$P_{\ell}^{4m}(0) = \begin{cases} 0, & \ell + 4m \text{ is odd} \Leftrightarrow \ell \text{ is odd} \\ \text{non-zero}, & \ell + 4m \text{ is even} \Leftrightarrow \ell \text{ is even} \end{cases}. \tag{12}$$

We obtain:

$$\begin{aligned} u_{\Sigma}^{f} &= 6u_0 j_0(k\Delta) + 2\sum_{\ell=1}^{\infty} j_{2\ell}(k\Delta) \left\{ a_{2\ell}^{0} + 2\sum_{m=0}^{\frac{\ell}{2}} \left[P_{2\ell}^{4m}(0)\, a_{2\ell}^{4m}\right] \right\}, \\ &= 6u_0 j_0(k\Delta) + 2j_2(k\Delta)\left[2P_2^0(0) + 1\right] a_2^0 \\ &\quad +2\sum_{\ell=2}^{\infty} j_{2\ell}(k\Delta) \left\{ a_{2\ell}^{0} + 2\sum_{m=0}^{\frac{\ell}{2}} \left[P_{2\ell}^{4m}(0)\, a_{2\ell}^{4m}\right] \right\}. \end{aligned} \tag{13}$$

We also know $P_2^0(0) = -1/2$. Thus,

$$u_{\Sigma}^{f} - [6j_0(k\Delta)]\, u_0 = O_{\text{LFE3D-7}},$$
$$O_{\text{LFE3D-7}} = 4\sum_{\ell=2}^{\infty} j_{2\ell}(k\Delta) \left\{ \frac{a_{2\ell}^{0}}{2} + \sum_{m=0}^{\left[\frac{\ell}{2}\right]} \left[P_{2\ell}^{4m}(0)\, a_{2\ell}^{4m}\right] \right\}. \tag{14}$$

Here $O_{\text{LFE3D-7}}$ is the truncation function for the simple compact LFE3D-7 formula.

$$W_f\, u_{\Sigma}^{f} + W_e\, u_{\Sigma}^{e} + W_c\, u_{\Sigma}^{c} - W_0 u_0 = 0,$$
$$W_f = \frac{1}{\Delta^2},\ \ W_e = 0,\ \ W_c = 0,\ \ W_0 = \frac{6j_0(k\Delta)}{\Delta^2}. \quad \text{(LFE3D-7)} \tag{15}$$

3.1.2. Step 2: LFE3D-13 (Edge-centered LFE)

Next we consider the twelve edge-centered fields using Eq. (7b). We further divide the twelve points into three sub-groups. We have, for points located on the $y = 0$ plane:

$$u_{+0+} = u_0 j_0\left(\sqrt{2}k\Delta\right) + \sum_{\ell=1}^{\infty} j_\ell\left(\sqrt{2}k\Delta\right) \sum_{m=0}^{\ell} \left[P_\ell^m\left(\frac{1}{\sqrt{2}}\right) a_\ell^m\right], \tag{16a}$$

$$u_{+0-} = u_0 j_0\left(\sqrt{2}k\Delta\right) + \sum_{\ell=1}^{\infty} j_\ell\left(\sqrt{2}k\Delta\right) \sum_{m=0}^{\ell} \left[P_\ell^m\left(\frac{-1}{\sqrt{2}}\right) a_\ell^m\right], \tag{16b}$$

$$u_{-0+} = u_0 j_0\left(\sqrt{2}k\Delta\right) + \sum_{\ell=1}^{\infty} j_\ell\left(\sqrt{2}k\Delta\right) \sum_{m=0}^{\ell} \left[(-1)^m P_\ell^m\left(\frac{1}{\sqrt{2}}\right) a_\ell^m\right], \tag{16c}$$

$$u_{-0-} = u_0 j_0\left(\sqrt{2}k\Delta\right) + \sum_{\ell=1}^{\infty} j_\ell\left(\sqrt{2}k\Delta\right) \sum_{m=0}^{\ell} \left[(-1)^m P_\ell^m\left(\frac{-1}{\sqrt{2}}\right) a_\ell^m\right]. \tag{16d}$$

For fields located on the $z = 0$ plane:

$$\begin{aligned} u_{++0} &= u_0 j_0\left(\sqrt{2}k\Delta\right) + \sum_{\ell=1}^{\infty} j_\ell\left(\sqrt{2}k\Delta\right) \sum_{m=0}^{\ell} P_\ell^m(0) \\ &\quad \left[a_\ell^m \cos\left(\frac{m\pi}{4}\right) + b_\ell^m \sin\left(\frac{m\pi}{4}\right)\right], \end{aligned} \tag{17a}$$

$$\begin{aligned} u_{-+0} &= u_0 j_0\left(\sqrt{2}k\Delta\right) + \sum_{\ell=1}^{\infty} j_\ell\left(\sqrt{2}k\Delta\right) \sum_{m=0}^{\ell} P_\ell^m(0) \\ &\quad \left[a_\ell^m \cos\left(\frac{3m\pi}{4}\right) + b_\ell^m \sin\left(\frac{3m\pi}{4}\right)\right], \end{aligned} \tag{17b}$$

$$\begin{aligned} u_{+-0} &= u_0 j_0\left(\sqrt{2}k\Delta\right) + \sum_{\ell=1}^{\infty} j_\ell\left(\sqrt{2}k\Delta\right) \sum_{m=0}^{\ell} P_\ell^m(0) \\ &\quad \left[a_\ell^m \cos\left(\frac{m\pi}{4}\right) - b_\ell^m \sin\left(\frac{m\pi}{4}\right)\right], \end{aligned} \tag{17c}$$

$$\begin{aligned} u_{--0} &= u_0 j_0\left(\sqrt{2}k\Delta\right) + \sum_{\ell=1}^{\infty} j_\ell\left(\sqrt{2}k\Delta\right) \sum_{m=0}^{\ell} P_\ell^m(0) \\ &\quad \left[a_\ell^m \cos\left(\frac{3m\pi}{4}\right) - b_\ell^m \sin\left(\frac{3m\pi}{4}\right)\right]. \end{aligned} \tag{17d}$$

And finally, for fields located on the $x = 0$ plane:

$$u_{0++} = u_0 j_0\left(\sqrt{2}k\Delta\right) + \sum_{\ell=1}^{\infty} j_\ell\left(\sqrt{2}k\Delta\right) \sum_{m=0}^{\ell} P_\ell^m\left(\frac{1}{\sqrt{2}}\right) \left[a_\ell^m \cos\left(\frac{m_\ell \pi}{2}\right) + b_\ell^m \sin\left(\frac{m_\ell \pi}{2}\right)\right], \tag{18a}$$

$$u_{0-+} = u_0 j_0\left(\sqrt{2}k\Delta\right) + \sum_{\ell=1}^{\infty} j_\ell\left(\sqrt{2}k\Delta\right) \sum_{m=0}^{\ell} P_\ell^m\left(\frac{1}{\sqrt{2}}\right) \left[a_\ell^m \cos\left(\frac{m\pi}{2}\right) - b_\ell^m \sin\left(\frac{m\pi}{2}\right)\right], \tag{18b}$$

$$u_{0+-} = u_0 j_0\left(\sqrt{2}k\Delta\right) + \sum_{\ell=1}^{\infty} j_\ell\left(\sqrt{2}k\Delta\right) \sum_{m=0}^{\ell} P_\ell^m\left(\frac{-1}{\sqrt{2}}\right) \left[a_\ell^m \cos\left(\frac{m\pi}{2}\right) + b_\ell^m \sin\left(\frac{m\pi}{2}\right)\right], \tag{18c}$$

$$u_{0--} = u_0 j_0\left(\sqrt{2}k\Delta\right) + \sum_{\ell=1}^{\infty} j_\ell\left(\sqrt{2}k\Delta\right) \sum_{m=0}^{\ell} P_\ell^m\left(\frac{-1}{\sqrt{2}}\right) \left[a_\ell^m \cos\left(\frac{m\pi}{2}\right) - b_\ell^m \sin\left(\frac{m\pi}{2}\right)\right]. \tag{18d}$$

We sum up the fields for each sub group to obtain:

$$u_{+0+} + u_{+0-} + u_{-0+} + u_{-0-} = 4u_0 j_0\Big(\sqrt{2}k\Delta\Big) + 2\sum_{\ell=1}^{\infty} j_\ell\Big(\sqrt{2}k\Delta\Big) \sum_{m=0}^{\left[\frac{\ell}{2}\right]} \left[P_\ell^{2m}\left(\frac{1}{\sqrt{2}}\right) + P_\ell^{2m}\left(\frac{-1}{\sqrt{2}}\right)\right] a_\ell^{2m}. \tag{19a}$$

$$u_{++0} + u_{+-0} + u_{-+0} + u_{--0} = 4u_0 j_0\Big(\sqrt{2}k\Delta\Big) + 2\sum_{\ell=1}^{\infty} j_\ell\Big(\sqrt{2}k\Delta\Big) \sum_{m=0}^{\ell} P_\ell^m(0) \left[\cos\left(\frac{m\pi}{4}\right) + \cos\left(\frac{3m\pi}{4}\right)\right] a_\ell^m, \tag{19b}$$

$$u_{0++} + u_{0+-} + u_{0-+} + u_{0--} = 4u_0 j_0\Big(\sqrt{2}k\Delta\Big) + 2\sum_{\ell=1}^{\infty} j_\ell\Big(\sqrt{2}k\Delta\Big) \sum_{m=0}^{\ell} \left[P_\ell^m\left(\frac{1}{\sqrt{2}}\right) + P_\ell^m\left(\frac{-1}{\sqrt{2}}\right)\right] \cos\Big(\frac{m_\ell \pi}{2}\Big) a_\ell^m. \tag{19c}$$

Next we apply the following properties for the associated Legendre polynomial:

$$P_\ell^m(z) \text{ is } \begin{cases} \text{odd}, & \text{if } m+\ell \text{ is odd} \\ \text{even}, & \text{if } m+\ell \text{ is even} \end{cases}. \tag{20a}$$

$$P_\ell^{2m}\left(\frac{1}{\sqrt{2}}\right) + P_\ell^{2m}\left(\frac{-1}{\sqrt{2}}\right) = \begin{cases} 0, & \ell \text{ is odd} \\ 2P_\ell^{2m}\left(\frac{1}{\sqrt{2}}\right), & \ell \text{ is even} \end{cases} \tag{20b}$$

$$P_\ell^{2m}\left(\frac{1}{\sqrt{2}}\right) + P_\ell^{2m}\left(\frac{-1}{\sqrt{2}}\right) = \begin{cases} 0, & \ell \text{ is odd} \\ 2P_\ell^{2m}\left(\frac{1}{\sqrt{2}}\right), & \ell \text{ is even} \end{cases}. \tag{20c}$$

Considering that:

$$\cos\left(\frac{m\pi}{4}\right) + \cos\left(\frac{3m\pi}{4}\right) = \begin{cases} 2(-1)^m, & m = 4k, \\ 0, & m \text{ otherwise}, \end{cases} \tag{21a}$$

$$\cos\left(\frac{m\pi}{2}\right) = \begin{cases} 1, & m = 4k, \\ 0, & m = 4k+1, \\ -1, & m = 4k+2, \\ 0, & m = 4k+3. \end{cases} \tag{21b}$$

we obtain:

$$\begin{aligned} u_\Sigma^e &= 12u_0 j_0\left(\sqrt{2}k\Delta\right) + 4\sum_{l=1}^{\infty} j_{2l}\left(\sqrt{2}k\Delta\right) \sum_{m=0}^{l}\left[P_{2l}^{2m}\left(\frac{1}{\sqrt{2}}\right) a_{2l}^{2m}\right] \\ &\quad +4\sum_{\ell=1}^{\infty} j_{2\ell}\left(\sqrt{2}k\Delta\right) \sum_{m=0}^{\left[\frac{\ell}{2}\right]}\left[(-1)^m P_{2\ell}^{4m}(0)\, a_{2\ell}^{4m}\right] \\ &\quad +4\sum_{\ell=1}^{\infty} j_{2\ell}\left(\sqrt{2}k\Delta\right) \sum_{m=0}^{l}\left[(-1)^m P_{2\ell}^{2m}\left(\frac{1}{\sqrt{2}}\right) a_{2\ell}^{2m}\right]. \end{aligned} \tag{22a}$$

We can further combine the second and the last term of the above equations to obtain:

$$\begin{aligned} u_\Sigma^e &= 12u_0 j_0\left(\sqrt{2}k\Delta\right) + 8\sum_{\ell=1}^{\infty} j_{2\ell}\left(\sqrt{2}k\Delta\right) \sum_{m=0}^{\left[\frac{l}{2}\right]}\left[P_{2\ell}^{4m}\left(\frac{1}{\sqrt{2}}\right) a_{2\ell}^{4m}\right] \\ &\quad +4\sum_{\ell=1}^{\infty} j_{2\ell}\left(\sqrt{2}k\Delta\right) \sum_{m=0}^{\frac{\ell}{2}}\left[(-1)^m P_{2\ell}^{4m}(0)\, a_{2\ell}^{4m}\right]. \end{aligned} \tag{22b}$$

Finally, we notice that the coefficient for $j_{2\ell}$ is $2P_2^0\left(1/\sqrt{2}\right) + P_2^0(0)$. These two terms happen to negate each other so we have the final

compact equation for sum of all edge fields as:

$$u_{\Sigma}^{e} = 12u_0 j_0\left(\sqrt{2}k\Delta\right) + 4\sum_{\ell=2}^{\infty} j_{2\ell}\left(\sqrt{2}k\Delta\right) \sum_{m=0}^{\frac{\ell}{2}}\left[2P_{2\ell}^{4m}\left(\frac{1}{\sqrt{2}}\right) + (-1)^m P_{2\ell}^{4m}(0)\right] a_{2\ell}^{4m}. \tag{22c}$$

This leads to the following edgepoint based LFE3D-13 formula:

$$W_f u_{\Sigma}^{f} + W_e u_{\Sigma}^{e} + W_c u_{\Sigma}^{c} - W_0 u_0 = 0,$$
$$W_f = 0,\ \ W_e = \frac{1}{\Delta^2},\ \ W_c = 0,\ \ W_0 = \frac{12 j_0\left(\sqrt{2}k\Delta\right)}{\Delta^2}, \quad \text{(LFE3D-13)} \tag{23a}$$

with the truncation function, $O_{\text{LFE3D-13}}$ given by:

$$O_{\text{LFE3D-13}} \triangleq u_{\Sigma}^{e} - 12 j_0\left(\sqrt{2}k\Delta\right) u_0 = 4\sum_{\ell=2}^{\infty} j_{2\ell}\left(\sqrt{2}k\Delta\right) \sum_{m=0}^{\frac{\ell}{2}}\left[2P_{2\ell}^{4m}\left(\frac{1}{\sqrt{2}}\right) + (-1)^m P_{2\ell}^{4m}(0)\right] a_{2\ell}^{4m}. \tag{23b}$$

3.1.3. Step 3: LFE3D-09 (Corner-point LFE)

We now turn to the focus on the contribution of the remaining eight corner fields. Using Eq. (7b) we have:

$$u_{+++} = u_0 j_0\left(\sqrt{3}k\Delta\right) + \sum_{\ell=1}^{\infty} j_{\ell}\left(\sqrt{3}k\Delta\right) \sum_{m=0}^{\ell} P_{\ell}^{m}\left(\frac{1}{\sqrt{3}}\right)\left(a_{\ell}^{m}\cos\frac{m\pi}{4} + b_{\ell}^{m}\sin\frac{m\pi}{4}\right), \tag{24a}$$

$$u_{++-} = u_0 j_0\left(\sqrt{3}k\Delta\right) + \sum_{\ell=1}^{\infty} j_{\ell}\left(\sqrt{3}k\Delta\right) \sum_{m=0}^{\ell} P_{\ell}^{m}\left(\frac{-1}{\sqrt{3}}\right)\left(a_{\ell}^{m}\cos\frac{m\pi}{4} + b_{\ell}^{m}\sin\frac{m\pi}{4}\right), \tag{24b}$$

$$u_{+-+} = u_0 j_0\left(\sqrt{3}k\Delta\right) + \sum_{\ell=1}^{\infty} j_{\ell}\left(\sqrt{3}k\Delta\right) \sum_{m=0}^{\ell} P_{\ell}^{m}\left(\frac{1}{\sqrt{3}}\right)\left(a_{\ell}^{m}\cos\frac{m\pi}{4} - b_{\ell}^{m}\sin\frac{m\pi}{4}\right), \tag{24c}$$

$$u_{+--} = u_0 j_0\left(\sqrt{3}k\Delta\right) + \sum_{\ell=1}^{\infty} j_\ell\left(\sqrt{3}k\Delta\right) \sum_{m=0}^{\ell} P_\ell^m\left(\frac{-1}{\sqrt{3}}\right)\left(a_\ell^m \cos\frac{m\pi}{4} - b_\ell^m \sin\frac{m\pi}{4}\right), \quad (24d)$$

and

$$u_{-++} = u_0 j_0\left(\sqrt{3}k\Delta\right) + \sum_{\ell=1}^{\infty} j_\ell\left(\sqrt{3}k\Delta\right) \sum_{m=0}^{\ell} P_\ell^m\left(\frac{1}{\sqrt{3}}\right)\left(a_\ell^m \cos\frac{3m\pi}{4} + b_\ell^m \sin\frac{3m\pi}{4}\right), \quad (25a)$$

$$u_{-+-} = u_0 j_0\left(\sqrt{3}k\Delta\right) + \sum_{\ell=1}^{\infty} j_\ell\left(\sqrt{3}k\Delta\right) \sum_{m=0}^{\ell} P_\ell^m\left(\frac{-1}{\sqrt{3}}\right)\left(a_\ell^m \cos\frac{3m\pi}{4} + b_\ell^m \sin\frac{3m\pi}{4}\right), \quad (25b)$$

$$u_{x^-y^-z^+} = u_0 j_0\left(\sqrt{3}k\Delta\right) + \sum_{\ell=1}^{\infty} j_\ell\left(\sqrt{3}k\Delta\right) \sum_{m=0}^{\ell} P_\ell^m\left(\frac{1}{\sqrt{3}}\right)\left(a_\ell^m \cos\frac{3m\pi}{4} - b_\ell^m \sin\frac{3m\pi}{4}\right), \quad (25c)$$

$$u_{x^-y^-z^-} = u_0 j_0\left(\sqrt{3}k\Delta\right) + \sum_{\ell=1}^{\infty} j_\ell\left(\sqrt{3}k\Delta\right) \sum_{m=0}^{\ell} P_\ell^m\left(\frac{-1}{\sqrt{3}}\right)\left(a_\ell^m \cos\frac{3m\pi}{4} - b_\ell^m \sin\frac{3m\pi}{4}\right). \quad (25d)$$

Summing up Eqs. (24a)–(25d), we have:

$$u_\Sigma^c = 8 j_0\left(\sqrt{3}k\Delta\right) u_0 + 4\sum_{\ell=1}^{\infty} j_\ell\left(\sqrt{3}k\Delta\right) \sum_{m=0}^{\left[\frac{\ell}{4}\right]} \left\{(-1)^m \left[P_\ell^{4m}\left(\frac{1}{\sqrt{3}}\right) + P_\ell^{4m}\left(\frac{-1}{\sqrt{3}}\right)\right] a_\ell^{4m}\right\}. \quad (26)$$

Next we apply the following properties for the associated Legendre polynomial:

$$P_\ell^{4m}\left(\frac{1}{\sqrt{3}}\right)+P_\ell^{4m}\left(\frac{-1}{\sqrt{3}}\right)=\begin{cases}0, & \ell \text{ is odd}\\ 2P_\ell^{4m}\left(\frac{1}{\sqrt{3}}\right), & \ell \text{ is even}\end{cases}, \tag{27a}$$

$$P_2^0\left(\frac{1}{\sqrt{3}}\right)=\frac{1}{2}\left(3\cos^2\theta-1\right)\Big|_{\theta=\cos^{-1}\left(\frac{1}{\sqrt{3}}\right)}=0. \tag{27b}$$

We have the final equation for the sum of all corner fields:

$$u_\Sigma^c=8j_0\left(\sqrt{3}k\Delta\right)u_0+8\sum_{\ell=2}^{\infty}j_{2\ell}\left(\sqrt{3}k\Delta\right)\sum_{m=0}^{\left[\frac{\ell}{2}\right]}\left[(-1)^m\,P_{2\ell}^{4m}\left(\frac{1}{\sqrt{3}}\right)a_{2\ell}^{4m}\right], \tag{28}$$

and the corner-point LFE3D-9 formula:

$$\begin{aligned}&W_f\,u_\Sigma^f+W_e\,u_\Sigma^e+W_c\,u_\Sigma^c-W_0u_0=0,\\ &W_f=0,\ \ W_e=0,\ \ W_c=\tfrac{1}{\Delta^2},\ \ W_0=\tfrac{8j_0\left(\sqrt{3}k\Delta\right)}{\Delta^2},\end{aligned}\qquad \text{(LFE3D-9)} \tag{29a}$$

with the truncation function, $O_{\text{LFE3D-9}}$ given by:

$$\begin{aligned}O_{\text{LFE3D-9}} &\triangleq u_\Sigma^c-8j_0\left(\sqrt{3}k\Delta\right)u_0\\ &=8\sum_{l=2}^{\infty}j_{2\ell}\left(\sqrt{3}k\Delta\right)\sum_{m=0}^{\left[\frac{\ell}{2}\right]}\left[(-1)^m\,P_{2\ell}^{4m}\left(\frac{1}{\sqrt{3}}\right)a_{2\ell}^{4m}\right].\end{aligned} \tag{29b}$$

3.1.4. Step 4: LFE3D-27 (All 26 Bordering Points Considered)

As mentioned earlier that LFE2D-9 equation can be derived from a linear combination of two LFE-5s equations along the plus and the cross coordinates so that the local error is minimized. So far to the best of our knowledge the only way to derive the sixth-order accurate LFE3D-27 formula is to look for the linear combination of LFE3D-07 (Eq. (15)), LFE3D-13 (Eq. (23a)) and LFE3D-09 (Eq. (29a)). We chose combinations that will reduce the local truncation error or global dispersion error. From the fact that the first leading term of the local truncation function for LFE2D-9 equation is the 8th-order Bessel function of the first kind, we suspect that the first leading term of the local truncation function for LFE3D-27 will be the 8th-order spherical Bessel function of the first kind. Closer examination of the three LFE3D truncation functions $O_{\text{LFE3D-07}}, O_{\text{LFE3D-13}}, O_{\text{LFE3D-09}}$ indicates that they all share two things in common: first the leading term function is the 4th-order spherical Bessel function of the first kind $j_4(k\Delta)$ and that they do not contain any odd term Bessel functions.

Hence we will focus on the elimination of both $j_4(k\Delta)$ and $j_6(k\Delta)$ terms.

From Eqs. (15), (23b), (29b) we know:

$$\begin{aligned} O_{\text{LFE3D-07}} &\triangleq u_{\Sigma}^{f} - 6j_0\left(k\Delta\right)u_0 \\ &= 4j_4\left(k\Delta\right)\left\{\left[\frac{1}{2}+P_4^0\left(0\right)\right]a_4^0 + P_4^4\left(0\right)a_4^4\right\} \\ &\quad +4j_6\left(k\Delta\right)\left\{\left[\frac{1}{2}+P_6^0\left(0\right)\right]a_6^0 + P_6^4\left(0\right)a_6^4\right\} \\ &\quad +O_{1h}\left((k\Delta)^8\right), \end{aligned} \tag{30a}$$

$$\begin{aligned} O_{\text{LFE3D-13}} &\triangleq u_{\Sigma}^{e} - 12j_0\left(\sqrt{2}k\Delta\right)u_0 \\ &= 4j_4\left(\sqrt{2}k\Delta\right)\left\{\left[2P_4^0\left(\frac{1}{\sqrt{2}}\right)+P_4^0\left(0\right)\right]a_4^0\right. \\ &\quad \left.+\left[2P_4^4\left(\frac{1}{\sqrt{2}}\right)-P_4^4\left(0\right)\right]a_4^4\right\} \\ &\quad +4j_6\left(\sqrt{2}k\Delta\right)\left\{\left[2P_6^0\left(\frac{1}{\sqrt{2}}\right)+P_6^0\left(0\right)\right]a_6^0\right. \\ &\quad \left.+\left[2P_6^4\left(\frac{1}{\sqrt{2}}\right)-P_6^4\left(0\right)\right]a_6^4\right\}+O_{2h}\left((k\Delta)^8\right), \end{aligned} \tag{30b}$$

$$\begin{aligned} O_{\text{LFE3D-09}} &\triangleq u_{\Sigma}^{c} - 8j_0\left(\sqrt{3}k\Delta\right)u_0 \\ &= 8j_4\left(\sqrt{3}k\Delta\right)\left[P_4^0\left(\frac{1}{\sqrt{3}}\right)a_4^0 - P_4^4\left(\frac{1}{\sqrt{3}}\right)a_4^4\right] \\ &\quad +8j_6\left(\sqrt{3}k\Delta\right)\left[P_6^0\left(\frac{1}{\sqrt{3}}\right)a_6^0 - P_6^4\left(\frac{1}{\sqrt{3}}\right)a_6^4\right] \\ &\quad +O_{3h}\left((k\Delta)^8\right). \end{aligned} \tag{30c}$$

The higher-order terms, O_{1h} in (30a), O_{2h} in (30b), and O_{3h} in (30c), are respectively defined as:

$$O_{1h}\left((k\Delta)^8\right) = 4\sum_{\ell=4}^{\infty} j_{2\ell}\left(k\Delta\right)\left\{\frac{a_{2\ell}^0}{2}+\sum_{m=0}^{\left[\frac{l}{2}\right]}\left[P_{2\ell}^{4m}\left(0\right)a_{2\ell}^{4m}\right]\right\} \tag{31a}$$

$$O_{2h}\left((k\Delta)^8\right) = 4\sum_{\ell=4}^{\infty} j_{2\ell}\left(\sqrt{2}k\Delta\right)$$

$$\sum_{m=0}^{\left[\frac{\ell}{2}\right]}\left[2P_{2\ell}^{4m}\left(\frac{1}{\sqrt{2}}\right)+(-1)^m P_{2\ell}^{4m}(0)\right]a_{2\ell}^{4m} \tag{31b}$$

$$O_{3h}\left((k\Delta)^8\right)=8\sum_{\ell=4}^{\infty}j_{2\ell}\left(\sqrt{3}k\Delta\right)\sum_{m=0}^{\left[\frac{\ell}{2}\right]}\left[(-1)^m P_{2\ell}^{4m}\left(\frac{1}{\sqrt{3}}\right)a_{2\ell}^{4m}\right]. \tag{31c}$$

The associated Legendre polynomials have following values:

$$\begin{cases} P_4^0(0)=\dfrac{3}{8}; \quad P_4^0\left(\dfrac{1}{\sqrt{2}}\right)=\dfrac{-13}{32}; \quad P_4^0\left(\dfrac{1}{\sqrt{3}}\right)=\dfrac{-7}{18} \\ P_4^4(0)=105; \quad P_4^4\left(\dfrac{1}{\sqrt{2}}\right)=\dfrac{105}{4}; \quad P_4^4\left(\dfrac{1}{\sqrt{3}}\right)=\dfrac{140}{3} \\ P_6^0(0)=\dfrac{-5}{16}; \quad P_6^0\left(\dfrac{1}{\sqrt{2}}\right)=\dfrac{-19}{128}; \quad P_6^0\left(\dfrac{1}{\sqrt{3}}\right)=\dfrac{2}{9} \\ P_6^4(0)=\dfrac{-945}{2}; \quad P_6^4\left(\dfrac{1}{\sqrt{2}}\right)=\dfrac{9\times 945}{16}; \quad P_6^4\left(\dfrac{1}{\sqrt{3}}\right)=560 \end{cases} \tag{32}$$

Substituting Eq. (32) into Eqs. (31a)–(31c) we will have:

$$\begin{aligned} O_{\text{LFE3D-07}} &= j_4(k\Delta)\left(\frac{7}{2}a_4^0+420a_4^4\right) \\ &\quad +j_6(k\Delta)\left(\frac{3}{4}a_6^0-1890a_6^4\right)+O_{1h}\left((k\Delta)^8\right), \end{aligned} \tag{33a}$$

$$\begin{aligned} O_{\text{LFE3D-13}} &= j_4\left(\sqrt{2}k\Delta\right)\left(\frac{-7}{4}a_4^0-210a_4^4\right) \\ &\quad +j_6\left(\sqrt{2}k\Delta\right)\left(\frac{-39}{16}a_6^0+\frac{13\times 945}{2}a_6^4\right)+O_{1h}\left((k\Delta)^8\right), \end{aligned} \tag{33b}$$

$$\begin{aligned} O_{\text{LFE3D-09}} &= j_4\left(\sqrt{3}k\Delta\right)\left(\frac{-28}{9}a_4^0-\frac{1120}{3}a_4^4\right) \\ &\quad +j_6\left(\sqrt{3}k\Delta\right)\left(\frac{16}{9}a_6^0-4480a_6^4\right)+O_{3h}\left((k\Delta)^8\right). \end{aligned} \tag{33c}$$

Let

$$\begin{cases} \alpha=\frac{28}{9}a_4^0+\frac{1120}{3}a_4^4 \\ \beta=\frac{2}{3}a_6^0-1680a_6^4 \end{cases}, \tag{34a}$$

and

$$\begin{cases} h_1=j_4(k\Delta) \\ h_2=j_4\left(\sqrt{2}k\Delta\right) \\ h_3=j_4\left(\sqrt{3}k\Delta\right) \end{cases}, \quad \begin{cases} q_1=j_6(k\Delta) \\ q_2=j_6\left(\sqrt{2}k\Delta\right) \\ q_3=j_6\left(\sqrt{3}k\Delta\right) \end{cases}. \tag{34b}$$

Substituting Eqs. (34a)–(34b) into Eqs. (33a)–(33b) we have:

$$O_{\text{LFE3D-07}} = h_1\left(\frac{9\alpha}{8}\right) + q_1\left(\frac{9\beta}{8}\right) + O_{1h}\left(\Delta^8\right), \tag{35a}$$

$$O_{\text{LFE3D-13}} = h_2\left(\frac{-9\alpha}{16}\right) + q_2\left(\frac{-117\beta}{32}\right) + O_{2h}\left(\Delta^8\right), \tag{35b}$$

$$O_{\text{LFE3D-09}} = h_3\left(-\alpha\right) + q_3\left(\frac{8\beta}{3}\right) + O_{3h}\left(\Delta^8\right). \tag{35c}$$

We now have the local truncation functions of the three LFE3D formulae. We are ready to combine them to obtain our LFE3D-27 equation. By denoting $C_1(k\Delta)$, $C_2(k\Delta)$ and $C_3(k\Delta)$ as the corresponding coefficient functions for the superpositioning of LFE3D-7, LFE3D-13 and LFE3D-9, we now construct the LFE3D-27 formula as follows:

$$C_1 u_\Sigma^f + C_2 u_\Sigma^e + C_3 u_\Sigma^c + C_0 u_0 = O_{\text{LFE3D-27}}. \tag{36}$$

Here $C_0(k\Delta)$ is given by:

$$\begin{aligned} C_0(k\Delta) = &-\left[6C_1(k\Delta)\, j_0(k\Delta)\right. \\ &\left. +12C_2(k\Delta)\, j_0\left(\sqrt{2}k\Delta\right) + 8C_3(k\Delta)\, j_0\left(\sqrt{3}k\Delta\right)\right], \end{aligned} \tag{37}$$

and the associated truncation function is given by:

$$O_{\text{LFE3D-27}} = C_1(k\Delta)\, O_{1h}\left(\Delta^8\right) + C_2(k\Delta)\, O_{2h}\left(\Delta^8\right) + C_3(k\Delta)\, O_{3h}\left(\Delta^8\right). \tag{38}$$

With a few steps omitted, we show the following must hold true:

$$\begin{aligned} &\alpha\left[\left(\frac{9h_1}{8}\right)C_1 + \left(\frac{-9h_2}{16}\right)C_2 + \left(-h_3\right)C_3\right] \\ &+\beta\left[\left(\frac{9q_1}{8}\right)C_1 + \left(\frac{-117q_2}{32}\right)C_2 + \left(\frac{8q_3}{3}\right)C_3\right] = 0. \end{aligned} \tag{39}$$

Because α and β (defined in Eq. (34a)) can not all be zero. Eq. (39) holds true if and only if:

$$\begin{aligned} \left(\frac{9h_1}{8}\right)C_1 + \left(\frac{-9h_2}{16}\right)C_2 + \left(-h_3\right)C_3 = 0, \\ \left(\frac{9q_1}{8}\right)C_1 + \left(\frac{-117q_2}{32}\right)C_2 + \left(\frac{8q_3}{3}\right)C_3 = 0. \end{aligned} \tag{40}$$

After solving for the above underdetermined equations, we have the following conditional equations for $C_1,\ C_2$ and C_3:

$$\begin{aligned} C_1 : C_2 : C_3 &= \begin{vmatrix} \frac{-9h_2}{16} & -h_3 \\ \frac{-117q_2}{32} & \frac{8q_3}{3} \end{vmatrix} : \begin{vmatrix} -h_3 & \frac{9h_1}{8} \\ \frac{8q_3}{3} & \frac{9q_1}{8} \end{vmatrix} : \begin{vmatrix} \frac{9h_1}{8} & \frac{-9h_2}{16} \\ \frac{9q_1}{8} & \frac{-117q_2}{32} \end{vmatrix} \\ &= \left(h_2q_3 + \frac{39}{16}h_3q_2 \right) : \left(\frac{3}{4}h_3q_1 + 2h_1q_3 \right) \\ &\quad : \left(\frac{351}{128}h_1q_2 - \frac{27}{64}h_2q_1 \right). \end{aligned} \tag{41}$$

One of the solutions for these coefficient functions is given as below:

$$\begin{aligned} C_1 &= j_4\left(\sqrt{2}k\Delta\right) j_6\left(\sqrt{3}k\Delta\right) + \frac{39}{16} j_4\left(\sqrt{3}k\Delta\right) j_6\left(\sqrt{2}k\Delta\right), \\ C_2 &= \frac{3}{4} j_4\left(\sqrt{3}k\Delta\right) j_6\left(k\Delta\right) + 2j_4\left(k\Delta\right) j_6\left(\sqrt{3}k\Delta\right), \\ C_3 &= \frac{351}{128} j_4\left(k\Delta\right) j_6\left(\sqrt{2}k\Delta\right) - \frac{27}{64} j_4\left(\sqrt{2}k\Delta\right) j_6\left(k\Delta\right). \end{aligned} \tag{42}$$

With these specific coefficients we arrive at the following LFE3D-27 formula — the discretized three dimensional Helmholtz equation:

$$\begin{aligned} &W_f^{\mathrm{LFE}} u_\Sigma^f + W_e^{\mathrm{LFE}} u_\Sigma^e + W_c^{\mathrm{LFE}} u_\Sigma^c - W_0^{\mathrm{LFE}} u_0 = 0, \\ &W_f^{\mathrm{LFE}} = j_4\left(\sqrt{2}k\Delta\right) j_6\left(\sqrt{3}k\Delta\right) + \frac{39}{16} j_4\left(\sqrt{3}k\Delta\right) j_6\left(\sqrt{2}k\Delta\right), \\ &W_e^{\mathrm{LFE}} = \frac{3}{4} j_4\left(\sqrt{3}k\Delta\right) j_6\left(k\Delta\right) + 2j_4\left(k\Delta\right) j_6\left(\sqrt{3}k\Delta\right), \\ &W_c^{\mathrm{LFE}} = \frac{351}{128} j_4\left(k\Delta\right) j_6\left(\sqrt{2}k\Delta\right) - \frac{27}{64} j_4\left(\sqrt{2}k\Delta\right) j_6\left(k\Delta\right), \\ &W_0^{\mathrm{LFE}} = 6j_0\left(k\Delta\right) W_f^{\mathrm{LFE}} + 12 j_0\left(\sqrt{2}k\Delta\right) W_e^{\mathrm{LFE}} \\ &\qquad\quad + 8 j_0\left(\sqrt{3}k\Delta\right) W_c^{\mathrm{LFE}}, \end{aligned} \tag{43a}$$

or

$$u_0 = \frac{W_f^{\mathrm{LFE}} u_\Sigma^f + W_e^{\mathrm{LFE}} u_\Sigma^e + W_c^{\mathrm{LFE}} u_\Sigma^c}{6j_0\left(k\Delta\right) W_f^{\mathrm{LFE}} + 12 j_0\left(\sqrt{2}k\Delta\right) W_e^{\mathrm{LFE}} + 8 j_0\left(\sqrt{3}k\Delta\right) W_c^{\mathrm{LFE}}}. \tag{43b}$$

(LFE3D-27)

We have also confirmed that the LFE3D-27 equation is accurate to the sixth-order (in $k\Delta$) and the leading term of the truncation function is $j_8(k\Delta)$, the 8th-order spherical Bessel function of the first kind.

4. STANDARDIZATION OF COEFFICIENTS

So far we have derived the LFE3D-27 equation which gives us a highly accurate 3D compact FD-FD stencil for the Helmholtz equation. However, one more issue remains: the discrete form of 3D Helmholtz operator of Eq. (1). Let L be the exact system operator of (1):

$$L = \nabla^2 + k^2 \tag{44}$$

The general discretized form of (1) constructed on the compact 27-point stencil can be expressed as:

$$A\left(W_0^{\text{LFE}}u_0 + W_f^{\text{LFE}}u_\Sigma^f + W_e^{\text{LFE}}u_\Sigma^e + W_c^{\text{LFE}}u_\Sigma^c\right) = 0. \tag{45}$$

Here A is a normalization constant. Eq. (45) is standardized if it satisfies:

$$\lim_{\Delta\to 0} A\left(W_0^{\text{LFE}}u_0 + W_f^{\text{LFE}}u_\Sigma^f + W_e^{\text{LFE}}u_\Sigma^e + W_c^{\text{LFE}}u_\Sigma^c\right) = Lu_0. \tag{46}$$

This is the same definition we used in the standardization process of LFE2D-9 [10]. Now we consider three classic finite difference schemes for discretizing the L operator. The first one is the second-order accurate, seven point stencil equation FD3D-2-07 as given below:

$$Lu_0 \approx \hat{L}_{\text{FD3D-2-07}}\{u_0\} = \frac{u_\Sigma^f - 6\left(1 - \frac{k^2\Delta^2}{6}\right)u_0}{\Delta^2}. \tag{47a}$$

The second one FD3D-2-13, is given by:

$$Lu_0 \approx \hat{L}_{\text{FD3D-2-13}}\{u_0\} = \frac{u_\Sigma^e - 12\left(1 - \frac{k^2\Delta^2}{3}\right)u_0}{4\Delta^2}. \tag{47b}$$

And the third one FD3D-2-9:

$$Lu_0 \approx \hat{L}_{\text{FD3D-2-09}}\{u_0\} = \frac{u_\Sigma^c - 8\left(1 - \frac{k^2\Delta^2}{2}\right)u_0}{4\Delta^2}. \tag{47c}$$

We compare these three equations with the corresponding second-order accurate LFE3D equations which we derived earlier in Eq. (14), (LFE3D-07), Eq. (23a) (LFE3D-13) and Eq. (29a) for LFE3D-09. We have:

$$Lu_0 \approx \hat{L}_{\text{LFE3D-07}}\{u_0\} = \frac{u_\Sigma^c - 6j_0(k\Delta)u_0}{\Delta^2}, \tag{48a}$$

$$Lu_0 \approx \hat{L}_{\text{LFE3D-13}}\{u_0\} = \frac{u_\Sigma^e - 12j_0\left(\sqrt{2}k\Delta\right)u_0}{4\Delta^2}, \tag{48b}$$

$$Lu_0 \approx \hat{L}_{\text{LFE3D-09}}\{u_0\} = \frac{u_\Sigma^c - 8j_0\left(\sqrt{3}k\Delta\right)u_0}{4\Delta^2}. \tag{48c}$$

Next we superimpose the forementioned three operators:

$$Lu_0 \approx \hat{L}_{\text{LFE3D-27}}\{u_0\} = A_1\hat{L}_{\text{LFE3D-07}}\{u_0\} + A_2\hat{L}_{\text{LFE3D-13}}\{u_0\} + A_3\hat{L}_{\text{LFE3D-09}}\{u_0\}. \tag{49}$$

We require that these coefficients must add up to one

$$A_1 + A_2 + A_3 = 1. \tag{50}$$

And that they must also retain the following ratio:

$$A_1 : A_2 : A_3 = W_f^{\text{LFE}} : 4\,W_e^{\text{LFE}} : 4\,W_c^{\text{LFE}}. \tag{51}$$

Thus, we have:

$$A_1 = \frac{W_f^{\text{LFE}}}{W}, \quad A_2 = \frac{4\,W_e^{\text{LFE}}}{W}, \quad A_3 = \frac{4\,W_c^{\text{LFE}}}{W}, \tag{52a}$$

and

$$W = W_f^{\text{LFE}} + 4\,W_e^{\text{LFE}} + 4\,W_c^{\text{LFE}}. \tag{52b}$$

From Eqs. (50)–(52), we have the standardized LFE3D-27 equation:

$$\hat{L}_{\text{LFE-27-3D}}\{u_0\} = A_0u_0 + A_1\,u_\Sigma^f + A_2u_\Sigma^e + A_3u_\Sigma^c, \tag{53a}$$

$$\begin{aligned} A_0 &= \frac{W_0^{\text{LFE}}}{\Delta^2 W}, \quad A_1 = \frac{W_f^{\text{LFE}}}{\Delta^2 W}, \\ A_2 &= \frac{W_e^{\text{LFE}}}{\Delta^2 W}, \quad A_3 = \frac{W_c^{\text{LFE}}}{\Delta^2 W}. \end{aligned} \tag{53b}$$

where W is previously defined in Eq. (52b).

5. RECONSTRUCTION FORMULA FOR LFE3D-27

Unlike the 2D-CLF a "straight forward" closed-form reconstruction formulae for CLF in the 3D case does not exist. In 3D-CLF cases, a local field the basic patch is a cube. Refereeing to Fig. 1, the size of the compact stencil will be twenty seven. On the boundary of the cube there are a total of twenty six points — six on the faces, twelve on the edges and eight on the vertices (corners). It is not an easy task to carry out the 3D LFE extension. We note that, there are only a total of twenty five terms in the truncated series of the spherical harmonics up the 4th order harmonics. With the last term, $j_4(kr)P_4^4(\cos\theta)\sin 4\phi$, not contributing to any of these neighboring points on the surface of the cube, we are faced with the problem of setting up 26 equations with 24 unknowns. As we look further into this subject, we discover that there are more terms which are linearly dependent on their lower-order terms when evaluated at these CLF controlling points on the cubic surface.

Consider the local field expressed by the linear combination of all SFB harmonics up the 8th order:

$$u(r,\theta,\phi)\approx a_0^0 j_0(kr)+\sum_{\ell=1}^{7} j_\ell\,(kr)\sum_{m=0}^{\ell} P_\ell^m\,(\cos\theta)(a_\ell^m\cos m\phi+b_\ell^m\sin m\phi). \tag{54}$$

There are all together 63 candidates. Among these the 37 dependent (marked in red strikethrough) and 26 independent terms and are listed below:

$$\begin{array}{cccccccccccccc}
a_0^0 & & & & & & & & & & & & & \\
a_1^0 & a_1^1 & b_1^1 & & & & & & & & & & & \\
a_2^0 & a_2^1 & b_2^1 & a_2^2 & b_2^2 & & & & & & & & & \\
a_3^0 & a_3^1 & b_3^1 & a_3^2 & b_3^2 & a_3^3 & b_3^3 & & & & & & & \\
a_4^0 & a_4^1 & b_4^1 & a_4^2 & b_4^2 & a_4^3 & b_4^3 & a_4^4 & b_4^4 & & & & & \\
a_5^0 & a_5^1 & b_5^1 & a_5^2 & b_5^2 & a_5^3 & b_5^3 & a_5^4 & b_5^4 & a_5^5 & b_5^5 & & & \\
a_6^0 & a_6^1 & b_6^1 & a_6^2 & b_6^2 & a_6^3 & b_6^3 & a_6^4 & b_6^4 & a_6^5 & b_6^5 & a_6^6 & b_6^6 & \\
a_7^0 & a_7^1 & b_7^1 & a_7^2 & b_7^2 & a_7^3 & b_7^3 & a_7^4 & b_7^4 & a_7^5 & b_7^5 & a_7^6 & b_7^6 & a_7^7 \quad b_7^7
\end{array} \tag{55}$$

The selection rules are: I, it must not be all zero on these 26 control points, II, it must be linearly independent with its lower-order cousins and III, there must be exactly 26 independent terms to form a square matrix. We expect that the analytical reconstruction formula based on these independent SFB harmonics, if derived, will be too complex to be practical. And thus we will resort to the following numerical inversion to obtain the 3D CLF reconstruction formula:

$$\begin{aligned}
u\,(r,\theta,\phi)\;\approx\; & a_0 j_0\,(kr)+\sum_{n=1}^{3}\sum_{m=0}^{n} a_n^m A_n^m\,(r,\theta,\phi)+\sum_{n=1}^{3}\sum_{m=1}^{n} b_n^m B_n^m\,(r,\theta,\phi) \\
& +a_4^0 A_4^0\,(r,\theta,\phi)+a_4^1 A_4^1\,(r,\theta,\phi)+a_4^2 A_4^2\,(r,\theta,\phi) \\
& +b_4^2 B_4^2\,(r,\theta,\phi)+a_4^4 A_4^4\,(r,\theta,\phi)+a_5^0 A_5^0\,(r,\theta,\phi) \\
& +a_5^1 A_5^1\,(r,\theta,\phi)+b_5^1 B_5^1\,(r,\theta,\phi)+a_6^0 A_6^0\,(r,\theta,\phi) \\
& +b_7^2 B_7^2\,(r,\theta,\phi)=\sum_{\mathrm{FC},\,j=1}^{6} C_j^{\mathrm{FC}}\,(r,\theta,\phi)\,u_j^{\mathrm{FC}} \\
& +\sum_{\mathrm{EC},\,j=1}^{12} C_j^{\mathrm{EC}}\,(r,\theta,\phi)\,u_j^{\mathrm{EC}}+\sum_{\mathrm{CR},\,j=1}^{8} C_j^{\mathrm{CR}}\,(r,\theta,\phi)\,u_j^{\mathrm{CR}},
\end{aligned} \tag{56a}$$

where

$$\begin{aligned}
A_n^m\,(r,\theta,\phi) &= j_n\,(kr)\,P_n^m\,(\cos\theta)\cos m\phi, \\
B_n^m\,(r,\theta,\phi) &= j_n\,(kr)\,P_n^m\,(\cos\theta)\sin m\phi.
\end{aligned} \tag{56b}$$

Thus, to find the local field with a given cube the best we can do is to numerically obtain by inverting the 26 by 26 matrix, the SFB coefficients from the nodal points on the surface of the cube.

6. COMPUTATION OF THE 3D FREE SPACE GREEN'S FUNCTION

Consider the 3-D Helmholtz equation with a point source located at origin ($r = 0$):

$$\left(\nabla^2 + k^2\right) G\left(x, y, z\right) = -\delta(r). \tag{57}$$

The analytic solution of Eq. (57) can be obtained by reducing it to the following one-dimensional differential equation in the spherical coordinate system:

$$\left[\frac{1}{r^2}\frac{d}{dr}\left(r^2\frac{d}{dr}\right) + k^2\right] G\left(r\right) = -\frac{\delta(r)}{4\pi r^2}, \quad G\left(r\right) = \frac{e^{-jkr}}{4\pi r}. \tag{58}$$

To test our LFE3D-27 stencil, we repeat the computation in 3D Cartesian coordinate system. Due to the central symmetry in this

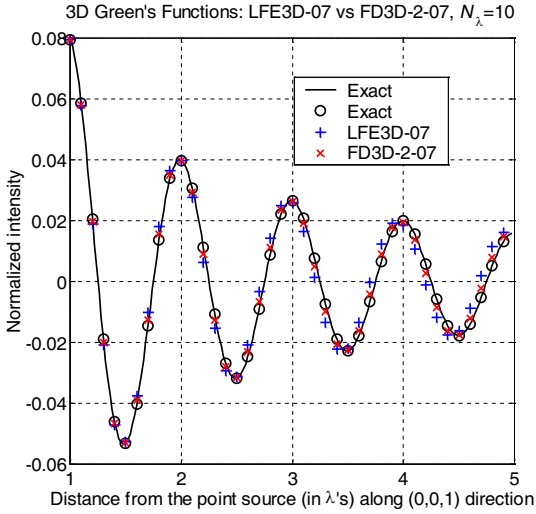

Figure 2. Comparison of 3D numerical Green's functions computed with LFE3D-07 and FD3D-2-07 stencils. The calibration point is located at $(0, 0, \lambda)$. The exact 3D Green's function solution is the continuous solid with circled points indicating the discrete field sampling location.

problem we compute only for the octant in the positive x, y and z-axes region. Evensymmetry boundary conditions are applied to planes $x = 0$, $y = 0$ and $z = 0$. The transparent/absorbing boundary conditions (TBC/ABC) are applied to the remaining three faces on the cube. A simple but effective impedance condition is applied to any point u_a on the ABC planes. When the location of the point source is known we may use the following expression for relating this field to its nearest corresponding fields u_{in} inside the computational domain:

$$u_a = u_{in} \left(\frac{r_{in}}{r_a} \right) \exp\left(-jk\left(r_a - r_{in}\right)\right). \tag{59}$$

where r_a is the distance from the said point to the origin and r_{in} the distance of the neighboring interior point to the origin. In our numerical experiments the point source is always located at the origin. Also the computed numerical and analytic Green's functions are normalized so that both are equal at a specific calibration point. We first computed and compared results between the classical second-order accurate FD3D-2-07 coefficient and the face-centered LFE3D-07 stencil. The solutions are plotted in Fig. 2. Starting from the calibration point, and at a sampling density of ten points per wavelength ($N_\lambda = 10$), to a distance of five wavelengths, both results are reasonably close to the solid curve of the exact solution. We also

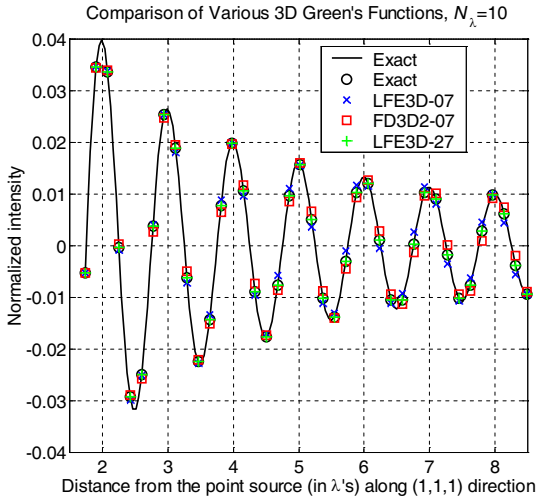

Figure 3. Comparison of 3D numerical Green's functions computed with LFE3D-07, FD3D2-07 and LFD3D-27 stencils. The calibration point is located at $(\lambda, \lambda, \lambda)$.

included the result from our LFE3D-27 formulation in Fig. 3 along the $(1, 1, 1)$ direction with the end point 8.5λ from the origin. In these calculations, there were up to a total of 125,000 unknowns (a cube containing 50 points in each dimension). This is the largest problem we can do with the 4G-DRAM on board. The linear equations are solved by a direct solver with our custom software which does its own virtual memory manipulation based on a block-tridiagonal LU factorizing scheme. The maximum run time is just under two minutes independent of whichever 3D compact stencil is used.

At a reduced sampling density $N_\lambda = 7$, results from LFE3D-07, FD3D2-07 begin to degrade as the field propagates away from the origin. However the sixth-order accurate FD3D6-27 results are still very accurate as we can see in Fig. 4 where the green plus points sit squarely in the black circles. As further reduced to a lower sampling density $N_\lambda = 5$, the results from LFE3D-07 are completely out of sync with the exact solution. We also see in Figs. 5 and 6, a clear deviation of the FD3D6-27 plus points from the exact circles near the end of the curves. However the results from our best 3D stencil LFE3D-27 are still correct as we see the red squares override the black circles.

At a much reduced sampling density $N_\lambda = 3$, results from FD3D6-27 begin to degrade soon after they travel away from the origin as can be seen in Figs. 7 and 8. Results from LFE3D-27 stencil are still quite acceptable as we see the red crosses are still tracking the black circles.

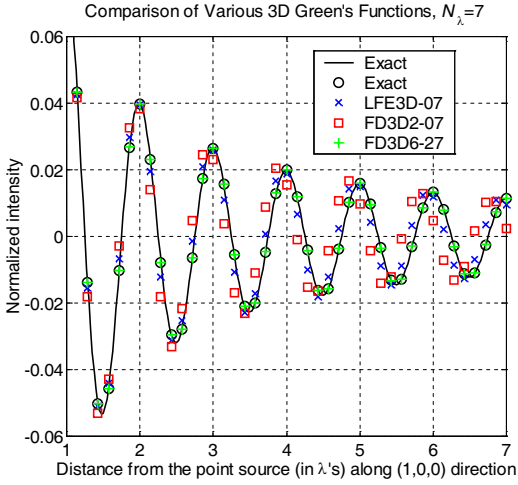

Figure 4. Comparison of 3D numerical Green's functions computed with LFE3D-07, FD3D2-07 and FD3D6-27 stencils at a reduced sampling density $N_\lambda = 7$. The calibration point is located at $(\lambda, 0, 0)$.

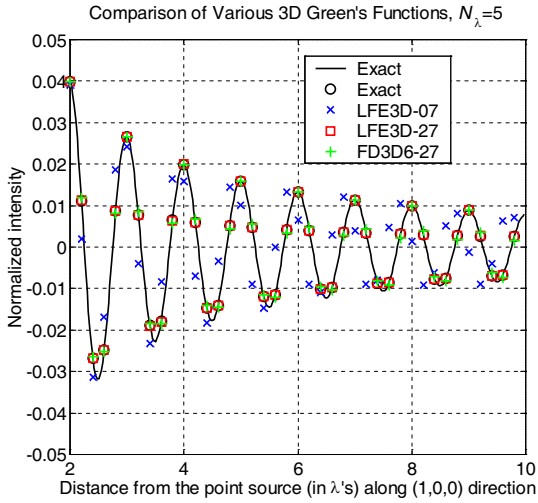

Figure 5. Comparison of 3D numerical Green's functions computed with LFE3D-07, FD3D6-27 and LFE3D-27 stencils at a low sampling density $N_\lambda = 5$. The calibration point is located at $(\lambda, 0, 0)$.

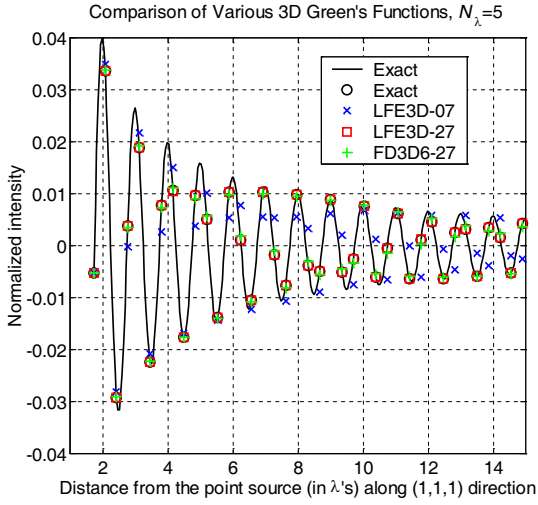

Figure 6. Same as Fig. 5 except for a new direction and a new calibration point at $(\lambda, \lambda, \lambda)$.

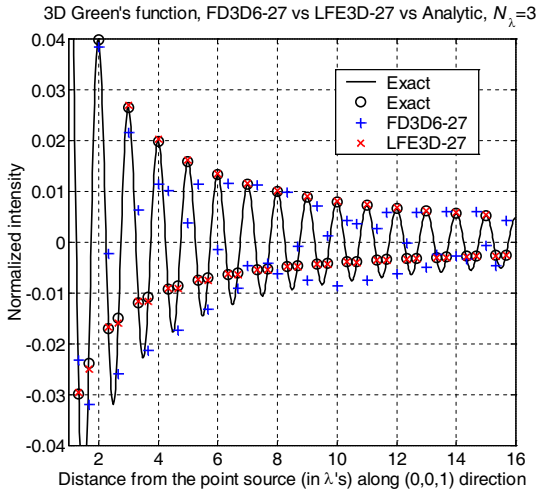

Figure 7. Comparison of 3D numerical Green's functions between FD3D6-27 and LFE3D-27. Results are computed at a very low sampling density $N_\lambda = 3$. The calibration point is located at $(0, 0, \lambda)$.

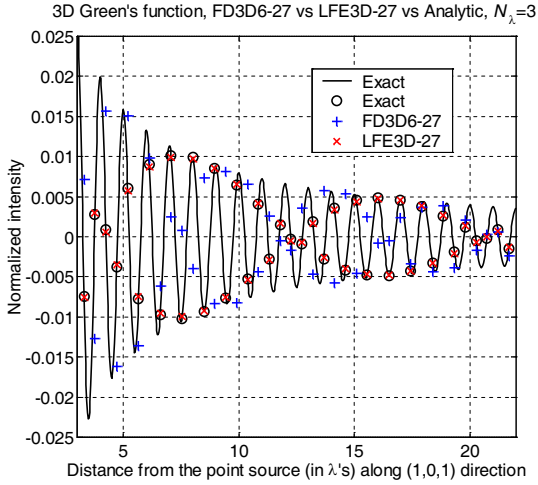

Figure 8. Same as Fig. 7 except for a new direction and a new calibration point at $(\lambda, 0, \lambda)$.

Finally, we ran the simulation at $N_\lambda = 2.5$, just for the sake of finding the threshold of our LFE3D-27 stencil. At this sampling density we are able to compute the 3D Green's function for a cube of twenty wavelengths in each dimension. We see from Fig. 9 that the red crosses are no longer sitting inside the black circles but they are still near-by.

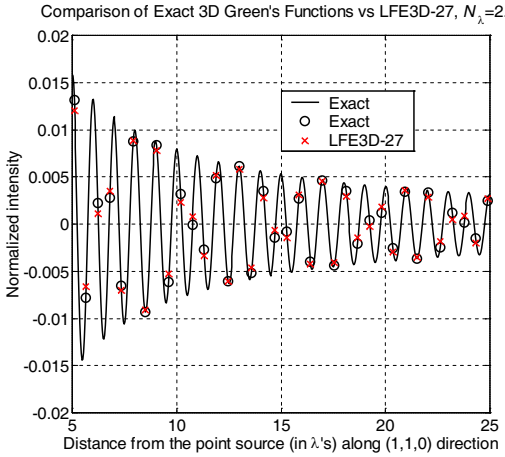

Figure 9. Results of 3D numerical Green's function of LFE3D-27 computed at 2.5 points per wavelength. The calibration point is located at $(\lambda, \lambda, 0)$.

7. DISCUSSIONS

While running these numerical experiments, we have discovered an interesting fact that one can not use the 3D LFE3D-09 or the LFE3D-13 stencil when one wishes to compute 3D fields due to a point excitation. These formulas are based on the edge/corner points only. These nodes are located further from the central point than those face-center ones. As a result, solutions of the numerical Green's function using LFE3D-09/LFE3D-13 formulation contain many zero fields all over the entire solution domain. Closer examination of the situation reveals that the disturbance propagates forward and backward "diagonally" causing unreachable gaps in the computational process of a single point-source. Hence the LFE3D-09 and LFE3D-13 stencils must be combined with the face-center LFE3D-07 stencil.

So far we have analytically derived the LFE3D-27, a SFB-based discrete form of the 3D Helmholtz operator in a homogeneous medium. We also investigated the accumulated amplitude and phase errors for this LFE3D-27 equation by numerically solving the 3-D Green's function and comparing it with the known analytic solution. There are many properties of this new formulation to be investigated. In a separate paper, we will derive an analytical expression for the local truncation error function of the standardized LFE3D-27 formula. The global error behavior will also be investigated via plane wave dispersion studies.

The recent advancements in highly accurate 2D FDFD algorithms enables us to simulate even larger and more complex 2-D problems. However, unlike 2-D cases, solving 3-D Helmholtz problems by FD-FD methods require solving significantly larger matrix equations. If N is the number of unknowns along an edge of a cube, a 3D FD-FD computation using a direct solver will have a storage requirement proportional to the fifth power of N and a computational cost proportional to the seventh power of N. In comparison, cost factors for a 3D FD-TD computation are reduced to N^3 for storage and N^4 for CPU. Some may argue that using an iterative sparse linear solver will help reduce the computational needs for 3D FD-FD methods. There are, unfortunately, no known robust iterative Helmholtz equation solvers [20]. That has been the reason why there were only a handful of applications in applying the FD-FD method to 3-D Helmholtz problems. This situation is about to change as we have seen from the 2D CLF dispersion analysis: at one percent phase error, the classical second-order accurate FD formulation requires a sampling density of twenty points per wavelength while 2D CLF requires only four. In 3D FD-FD calculation, this five-factor reduction in linear sampling density will translate to a factor of eighty thousand (five to the seventh power) in computational time cost saved. Such significant savings makes 3D CLF-based EM field simulations practical in some 3D EM applications.

There are still many lingering CLF related issues waiting to be solved. We have only considered the homogeneous case for the 3D Helmholtz equation. For complex passive optical waveguide/device problems we have to consider 3D EM wave fields in inhomogeneous media. We need to develop special LFE3D-27 stencils for cells near a dielectric interface. We also have to consider a vector formulation for 3D structures containing dielectric interfaces with large index contrasts. The method of connected local fields is still in an early stage of development, and requires further research before it becomes a viable tool for modeling 3D complex dielectric devices.

8. CONCLUSIONS

We have advanced the method of connected local fields to the three-dimensional case for obtaining semi-analytical solutions of Helmholtz equation. The fundamental building block in this 3-D CLF is a cube made of twenty seven points. By expanding the local field with a truncated spherical Fourier-Bessel series we develop closed-form, 3-D local field expansion coefficients called LFE3D-27. We also show that this novel formula has a very small local truncation error of the eighth-order. As in the 2D CLF, we are able to keep this 3D CLF structurally

equivalent to a standard 3-D FD-FD formulation using a compact 27-point stencil. With the development of the inhomogeneous 3D CLF method complete, all existing 3D FD-FD software can be modified with minimal effort to benefit from this new memory and CPU saving semi-analytical approach for solving the Helmholtz equation.

ACKNOWLEDGMENT

We are grateful for the support of the National Science Council of the Republic of China under the contracts NSC 101-2221-E-110-073.

REFERENCES

1. Chang, H.-W., Y.-H. Wu, and W.-C. Cheng, "Hybrid FD-FD analysis of crossing waveguides by exploiting both the plus and the cross structural symmetry," *Progress In Electromagnetics Research*, Vol. 103, 217–240, 2010.
2. Yu, C.-P. and H. C. Chang, "Compact finite-difference frequency-domain method for the analysis of two-dimensional photonic crystals," *Optics Express*, Vol. 12, 1397–1408, 2004.
3. Smith, G. D., *Numerical Solution of Partial Differential Equations*, 2nd edition, Oxford University Press, 1978.
4. Jo, C.-H., C. Shin, and J. H. Suh, "An optimal 9-point, finite-difference, frequency-space, 2-D scalar wave extrapolator," *Geophysics*, Vol. 61, 529–537, 1996.
5. Smith, G. D., *Numerical Solution of Partial Differential Equations*, 2nd edition, Oxford University Press, 1978.
6. Hadley, G. R., "High-accuracy finite-difference equations for dielectric waveguide analysis I: Uniform regions and dielectric interfaces," *Journal of Lightwave Technology*, Vol. 20, No. 7, 1219–1231, 2002.
7. Hadley, G. R., "High-accuracy finite-difference equations for dielectric waveguide analysis II: Dielectric corners," *Journal of Lightwave Technology*, Vol. 20, No. 7, 1210–1218, 2002.
8. Tsukerman, I., "Electromagnetic applications of a new finite-difference calculus," *IEEE Transactions on Magnetics*, Vol. 41, No. 7, 2206–2225, 2005.
9. Singer, I. and E. Turkel, "Sixth order accurate finite difference schemes for the Helmholtz equation," *Journal of Computational Acoustics*, Vol. 14, 339–351, 2006.

10. Chang, H.-W. and S.-Y. Mu, "Semi-analytical solutions of the 2-D homogeneous Helmholtz equation by the method of connected local fields," *Progress In Electromagnetics Research*, Vol. 109, 399–424, 2010.
11. Mu, S.-Y. and H.-W. Chang, "Theoretical foundation for the method of connected local fields," *Progress In Electromagnetics Research*, Vol. 114, 67–88, 2011.
12. Young, D. M. and J. H. Dauwalder, *Discrete Representations of Partial Differential Equations, Errors in Digital Computation*, Academic Press, New York, 1965
13. Sutmann, G., "Compact finite difference schemes of sixth order for the Helmholtz equation," *Journal of Computational and Applied Mathematics*, Vol. 203, 15–31, 2007.
14. Fernandes, D. T. and A. F. D. Loula, "Quasi optimal finite difference method for Helmholtz problem on unstructured grids," *Int. J. Numer. Meth. Engng.*, Vol. 82, 1244–1281, 2010.
15. Chang, H.-W. and S.-Y. Mu, "3-D LFE-27 formulae for the method of connected local fields," OPTIC-2012, OB-SA-BL1, Taipei, Taiwan, 2012.
16. Hall, C. A. and T. A. Porsching, *Numerical Analysis of Partial Differential Equations*, 248–250, Prentice-Hall, Englewood Cliffs, New Jersey, 1990.
17. Harari, I. and E. Turkel, "Accurate finite difference methods for time-harmonic wave propagation," *Journal of Computational Physics*, Vol. 119, No. 2, 252–270, 1995.
18. Spotz, W. F. and G. F. Carey, "A high-order compact formulation for the 3D Poisson equation," *Numerical Methods for Partial Differential Equations*, Vol. 12, No. 2, 235–243, 1996.
19. Nehrbass, J. W., J. O. Jevtic, and R. Lee, "Reducing the phase error for finite-difference methods without increasing the order," *IEEE Transactions on Antennas and Propagation*, Vol. 46, 1194–1201, 1998.
20. Ernst, O. G. and M. J. Gander, "Why it is difficult to solve Helmholtz problems with classical iterative methods," *Lecture Notes in Computational Science and Engineering,* Vol. 83, 325–363, 2012.